Chem Soc Rev

Tellurene, its physical properties, scalable nanomanufacturing, and device applications

Journal:	*Chemical Society Reviews*
Manuscript ID	CS-REV-07-2018-000598
Article Type:	Tutorial Review
Date Submitted by the Author:	25-Jul-2018
Complete List of Authors:	Wu, Wenzhuo; Purdue University, School of Industrial Engineering Qiu, Gang; Purdue University Wang, Yixiu; Purdue University, Wang, Ruoxing; Purdue University Ye, Peide; Purdue University, School of ECE

Chem Soc Rev

Tutorial Review

Tellurene, its physical properties, scalable nanomanufacturing, and device applications

Received 00th January 20xx,
Accepted 00th January 20xx

DOI: 10.1039/x0xx00000x

www.rsc.org/

Wenzhuo Wu,*[a, b, c, d] Gang Qiu,[c, e] Yixiu Wang,[a, b, c] Ruoxing Wang,[a, b, c] and Peide Ye*[c, e]

Tellurium (Te) has a trigonal crystal lattice with inherent structural anisotropy. Te is multifunctional, e.g., semiconducting, photoconductive, thermoelectric, piezoelectric, etc., for applications in electronics, sensors, optoelectronics, and energy devices. Due to the inherent structural anisotropy, previously reported synthetic methods predominantly yield one-dimensional (1D) Te nanostructures. Much less is known about the 2D Te nanostructures, their processing schemes, and material properties. This review focuses on the synthesis and morphology control of emerging 2D tellurene and summarizes the latest developments in understanding the fundamental properties of monolayer and few-layer tellurene, as well as the recent advances in demonstrating prototypical tellurene devices. Finally, the prospects for future research and application opportunities as well as the accompanying challenges of 2D tellurene are summarized and highlighted.

Key learning points
(1) Design and scalable-synthesis of 2D tellurene with controlled yield and dimensions.
(2) Key physical properties of 2D tellurene.
(3) Application of 2D tellurene in nanoelectronics: field-effect transistors.

1. Introduction

Group VI tellurium (Te) belongs to the chalcogen element family and is chemically related to selenium and sulfur. Its rarity in the earth's crust is comparable to that of platinum, while tellurium is far more common in the universe. Te has appealing properties, e.g., semiconducting[1], photoconductivity[2], thermoelectricity[3], topological property[4], and acoustic-optic property[5] for applications in electronics, sensors, optoelectronics, and energy devices. Te is also a crucial component of many functional materials, e.g., tellurides, for numerous societally-pervasive technologies, such as photovoltaics, thermoelectric devices, infrared imaging, etc. The bulk Te has a trigonal crystal lattice in which individual helical chains of Te atoms are stacked together by weak bonding and spiral around axes parallel to the [0001] direction at the center and corners of the hexagonal elementary cell[6] (Fig. 1a). Each tellurium atom is covalently bonded with its two nearest neighbors on the same chain.

Due to the inherent structural anisotropy, previously reported synthetic methods predominantly yield one-dimensional (1D) Te nanostructures[7-9]. Much less is known about the 2D Te nanostructures, their processing schemes, and material properties. As one of the newest members of the 2D materials' family, the existence of tellurene, in its monolayer or few-layer form, has only been recently confirmed by experimental work[10-13] and theoretical calculations[14, 15]. Inspired by the limited number of experimental studies available to date, there have been a few recent theoretical explorations[16-23] which predict the intriguing properties of 2D tellurene, e.g., extraordinary carrier mobility, significant optical absorption, high stretchability, etc.

In the following sections of this review, we intend to summarize and highlight the recent theoretical and experimental advances in studying 2D tellurene. Firstly, we will briefly review the progress in synthesizing Te nanostructures since the knowledge gained from these prior efforts provide valuable insights and guidance for the synthesis of 2D tellurene. Secondly, we will review and discuss the up-to-date understandings of the intriguing properties of 2D tellurene. The recent demonstration of the tellurene devices, e.g., transistor, will also be discussed. Lastly but not the least, we will provide our outlook and perspectives for the future opportunities and challenges in the research and application of 2D tellurene. It is expected that the intriguing, versatile material properties and technological potential of tellurene would open up numerous exciting opportunities in both the fundamental exploration and technological application of tellurene.

2. Synthesis of tellurium nanostructures

2.1 Synthesis of one-dimensional Te nanostructures

A wealth of synthetic methods has been developed to derive Te nanostructures with various morphologies during the past two decades, e.g., through solution phase reactions[7-9, 24, 25] and vapor

[a] School of Industrial Engineering, Purdue University, West Lafayette, Indiana 47907, USA. Email: wenzhuowu@purdue.edu
[b] Flex Laboratory, Purdue University, West Lafayette, Indiana 47907, USA.
[c] Birck Nanotechnology Center, Purdue University, West Lafayette, Indiana 47907, USA.
[d] Regenstrief Center for Healthcare Engineering, Purdue University, West Lafayette, Indiana 47907, USA.
[e] School of Electrical and Computer Engineering, Purdue University, West Lafayette, Indiana 47907, USA. Email: yep@purdue.edu

phase deposition[26, 27]. The products from these synthetic efforts are dominantly 1D nanostructures, such as nanowires, nanotubes, and nanobelts, growing along the [0001] chiral-chain direction because of the inherent structural anisotropy in tellurium[6] (Fig. 1).

2.1.1 Vapor-phase processes

Furuta and co-authors pioneered the synthesis of Te whiskers with a few microns in length through the sublimation of metallic Te on the solid substrates using a vapor-solid (VS) process at various temperatures, and have investigated the morphology evolution of the Te whiskers and the roles of the substrate temperature as well as the axial dislocation in related processes[28]. They further explored the growth of Te whiskers by a vapor-liquid-solid (VLS) process using various metal catalysts, e.g., Tl, Zn, and Se[29]. Later, Geng *et al.* demonstrated a chemical vapor deposition process for synthesizing 1D Te nanobelts by reacting Al_2Te_3 powder with H_2O in a horizontal tube furnace at 500 °C[30]. A few studies have also been reported on the growth of 1D Te nanostructures by physical vapor deposition. For example, Li and colleagues used the physical evaporation method to prepare the hollow prismatic Te microtubes, showing that the reaction

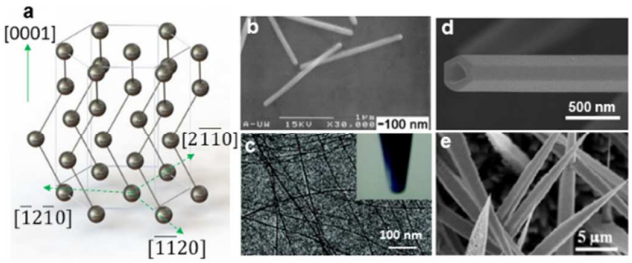

Figure 1 (a) The crystal structure of tellurium. (b)-(d) The various 1D Te nanostructures shown in previous reports through (b) solution phase synthesis. Reproduced with permission from ref. 7. Copyright 2002, Royal Society of Chemistry. (c) PVP-assisted hydrothermal growth. Reproduced with permission from ref. 9. Copyright 2006, American Chemical Society. (d) hydrothermal reduction method. Reproduced with permission from ref. 8. Copyright 2002, WILEY-VCH Verlag GmbH & Co. KGaA, Weinheim. (e) physical vapor deposition process. Reproduced with permission from ref. 26. Copyright 2013, IOP Publishing.

temperature and the gas flow rate played critical roles in the growth control[27]. Employing a VS mechanism, He and co-authors reported a catalyst-free physical vapor deposition process for growing aligned 1D Te nanostructures with certain control over the nucleation density, size, and structures of the formed materials[26].

2.1.2 Solution-phase processes

The requirement for high growth temperature and delicate control in the growth atmosphere limit the scale-up potential of the vapor-phase approaches. In contrast, the solution-phase synthetic routes are more relevant for the potential large-scale synthesis of Te nanomaterials and have attracted numerous attentions during the past two decades. For example, Xia and colleagues reported the first synthesis of 1D trigonal-Te (*t*-Te) nanowires through a solution-phase, self-seeding process where the orthotelluric acid or tellurium dioxide was reduced by hydrazine at various refluxing temperatures[7]. Qian and co-workers subsequently reported the hydrothermal synthesis of Te nanobelts through the disproportionation of sodium tellurite (Na_2TeO_3) in aqueous ammonia solution[8] and revealed that the reaction parameters such as pH, temperature, and precursor concentration dictate the formation of the Te nanobelts. Yu and colleagues reported the large-scale synthesis of Te nanowires and nanobelts with uniform morphologies and high yield through a poly (vinyl pyrrolidone) (PVP)-assisted hydrothermal process[9]. Inspired by these early work, to date, the solution-based strategies for synthesizing 1D Te nanostructures typically rely on the reduction of a Te precursor in the presence of a surfactant, e.g., PVP or cetyltrimethyl ammonium bromide (CTAB). The morphology control for the product material strongly depends on the nucleation and growth conditions, such as the choice of surfactants, pH values, precursors, reaction time and so on. A comprehensive review of the solution-phase synthesis of Te nanostructures has been recently provided by Yu and colleagues[31]. The morphology-selective synthesis of 1D Te nanomaterials demonstrated in these prior work suggested that the surfactant-assisted modulation of the growth rates of relevant crystalline planes could be utilized to precisely control the reaction kinetics, and potentially enable the further morphology engineering of the as-synthesized Te nanomaterials.

2.2 Prior efforts in preparing 2D Te nanostructures

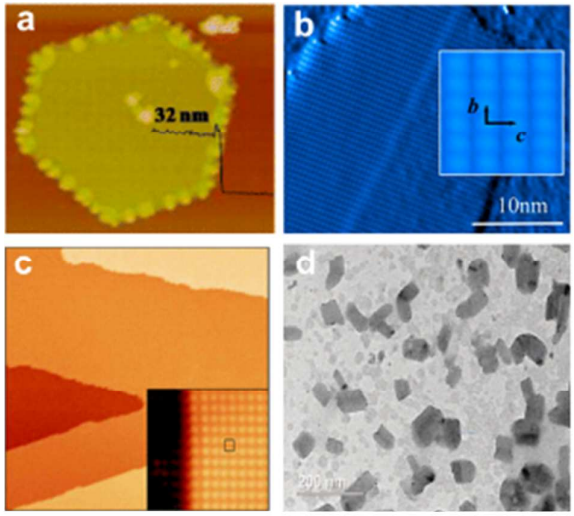

Figure 2 Previously reported 2D Te materials. (a) vdWE-grown hexagonal Te nanoplates. Reproduced with permission from ref. 32. Copyright 2014, American Chemical Society. (b) vdWE-grown monolayer and few-layer tellurene on graphene/6H-SiC(0001) substrate. Reproduced with permission from ref. 13. Copyright 2017, American Chemical Society. (c) Epitaxial Te thin film on HOPG substrate. Reproduced with permission from ref. 33. Copyright 2017, Royal Society of Chemistry. (d) Liquid-phase exfoliated Te nanocrystals. Reproduced with permission from ref. 34. Copyright 2017, WILEY-VCH Verlag GmbH & Co. KGaA, Weinheim.

In contrast to the fruitful progress achieved in synthesizing 1D Te nanostructures, much less is known about the 2D Te nanostructures, their processing schemes, and related properties. He and colleagues reported the synthesis of 2D hexagonal Te nanoplates (Fig. 2a) on the chemically inert surface of mica through the van der Waals epitaxy (vdWE)[32], during which the grown materials and the substrate are bonded by the weak vdW interaction. The derived 2D Te nanoplates in He's report have small lateral dimensions (6-10 μm), large thickness (30-80 nm), and non-uniform surface/edge roughness[32]. The substantial thickness of these Te nanoplates is well beyond the atomic scale and may diminish their potential material relevance and interests for the fundamental exploration and technological application in the 2D limit. Huang and colleagues recently reported the vdWE of monolayer and

few-layer Te films on graphene/6H-SiC(0001) substrate by molecular beam epitaxy (Fig. 2b)[13]. The authors identified that the epitaxy Te films consist of in-plane helical Te chains, which is different from the structures of Te nanoplates in the study of He and colleagues[32] as well as the structural models theoretically proposed for monolayer tellurene[14]. Chen and co-authors also demonstrated the growth of epitaxial Te thin films on highly oriented pyrolytic graphite (HOPG) substrates (Fig. 2c)[33] with a higher growth rate and a higher substrate temperature than that used in Huang's work[13]. In addition to these efforts in the epitaxial growth of Te thin films, Zhang and colleagues recently reported the liquid-phase exfoliation of Te nanocrystals with small lateral dimensions (~ 100 nm) (Fig. 2d)[34].

It should be noted that these demonstrated efforts in preparing 2D Te nanostructures are limited by the difficulty in deriving large-scale monolayer or few-layer 2D Te with uniform thickness, restrictions in the growth substrates and conditions (e.g., high temperature, vacuum), and the vague potential in scaling-up. For instance, the top-down liquid-phase exfoliation show potential in producing large quantities of Te nanocrystals. Nevertheless, the poor control in thickness uniformity and the small size of the derived materials undermine the viability of such approaches. The epitaxy approaches are also proved challenging, in particular for device implementation, due to the process-inherent demands for high growth temperature, delicate control in growth atmosphere, pressure and the epitaxy substrates. There has been a lack of feasible synthetic strategies for the scalable, substrate-free production of large-area, single-crystal 2D Te with process-tunable structural and material properties. Such fundamental knowledge and technological capability are essential for exploring the intriguing properties of 2D Te and implementing related device technologies.

2.3 Scalable solution synthesis of large-area free-standing 2D tellurene

To address these challenges, Wu and colleagues developed a substrate-free solution process to synthesize for the first time large-area, free-standing, high-quality monolayer, and few-layer tellurene crystals (Fig. 3)[10]. The samples were grown through the reduction of sodium tellurite (Na_2TeO_3) by hydrazine hydrate (N_2H_4) in an alkaline solution at temperatures from 160-200 ^{o}C, with the presence of crystal-face-blocking ligand PVP. Due to the substrate-free nature of the process and the use of the aqueous solution in the reaction, the 2D Te flakes can be transferred and assembled at large scale, through a Langmuir-Blodgett process onto various substrates for characterization and device integration. The derived 2D Te flakes from this process have edge lengths ranging from 50 to 100 μm, and thicknesses from a monolayer to tens of nm (Fig. 3a). Structural and material characterizations of all the 2D Te samples indicate that all samples grow laterally along the <0001> and <$1\bar{2}10$> directions, with the vertical stacking along the <$10\bar{1}0$> directions. This is the first experimental realization of large-area, free-standing, high-quality 2D Te crystals through a low-temperature, scalable substrate-free solution process.

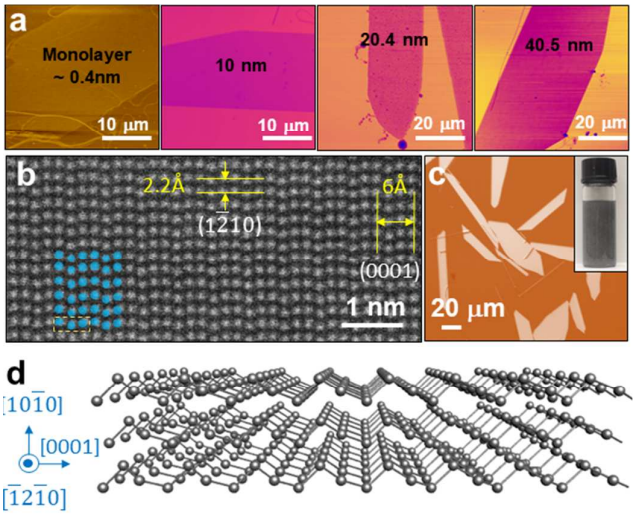

Figure 3 (a) AFM images of 2D Te with different thickness; (b) STEM image of the few-layer tellurene lattice; (c) Optical image of 2D Te. Inset: dispersed 2D Te solution; (d) 3D illustration of few-layer tellurene's structure. Reproduced with permission from ref. 10. Copyright 2018, Springer Nature.

The authors further systematically studied and revealed the synthetic pathway for deriving the 2D tellurene through the solution process. The controlled PVP concentration is the key to obtaining 2D tellurene. A closer examination of reactions with different PVP concentrations reveals an intriguing morphology evolution in growth products with time. For each PVP concentration, the initial growth products are dominantly 1D nanostructures, similar to previous reports[7-9]. After a certain period of reaction, structures possessing both 1D and 2D characteristics start to emerge. Finally, the ratio of 2D tellurene flakes which have a straight {$1\bar{2}10$} edge increases with a reduction in 1D and intermediate structures and reaches a plateau after an extended growth. The observed morphology evolution suggests that the balance between the kinetic and thermodynamic growth dictates the transformation from 1D structures to 2D forms. In the initial reaction, PVP is preferentially adsorbed on the {$10\bar{1}0$} surfaces of the nucleated seeds[9], which promotes the kinetic-driven 1D growth. When the growth continues, the {$10\bar{1}0$} surfaces of the formed structures become partially covered due to the insufficient PVP capping. Since {$10\bar{1}0$} surfaces have the lowest free energy in tellurium, the growth of {$10\bar{1}0$} surfaces along the <$1\bar{2}10$> direction significantly increases through the thermodynamic-driven assembly, leading to the 1D/2D intermediate structures. Wu and colleagues further demonstrated the engineering and optimization over the production yield of the process, and the dimensions and thicknesses of tellurene. Such capability in materials synthesis enables potential modulation of device performance through tuning the electronic structures, e.g., a process-tunable bandgap (0.3-1 eV) covering the spectral range from mid-infrared to near-infrared in tellurene.

3. Physical properties of tellurene

Tellurene is an emerging member of the 2D materials' family, and there has been only a few experimental work[10-13] and theoretical calculations[14, 16-23]. More advances are expected to occur from the efforts of the material research community in probing the fundamental properties of the emerging 2D tellurene and implementing novel devices.

3.1 Structural phase transition in monolayer and few-layer tellurene

Recent theoretical calculations suggest that, at equilibrium under normal conditions, the α-phase derived from the bulk trigonal structure is the most stable phase for few-layer tellurene[16] (Fig. 4), and the tetragonal β-phase is more stable for the monolayer tellurene due to the structural relaxation[14] (Fig. 4). The recent experimental efforts in deriving atomically-thin 2D Te also provide interesting and insightful results. The vdWE monolayer Te film grown by Chen and co-authors on highly oriented pyrolytic graphite (HOPG) substrates[33] have a crystal structure and in-plane lattice constants consistent with the predicted β-phase[14]. Nevertheless, the vdWE monolayer Te films grown on graphene layer, as reported by Huang and colleagues[13], were characterized to have a larger lattice of 4.42 × 5.93 Å^2 more consistent with the bulk trigonal configuration, where parallel-packed Te helical chains are flat-lying in the substrate plane. The structural characterizations in Wu and colleagues' work[10] confirmed that these solution-grown, free-standing few-layer tellurene crystals possess the bulk trigonal structure (Fig. 3). This is consistent with Ji and colleagues' calculation results that α-phase derived from the bulk trigonal structure is the most stable phase for few-layer tellurene[16]. The structural discrepancy seen in the 2D tellurium derived from different processes suggests the complexity of the underlying mechanism that drives the structure formation of monolayer or few-layer tellurene, and necessitates the devotion of more efforts in advancing both the theoretical understanding and the experimental investigation of the atomically-thin 2D tellurium, e.g., the roles of growth kinetics on its fundamental structural phase transition. Moreover, the substrate is expected to also play a critical role in dictating the structure and properties of the supported tellurene.

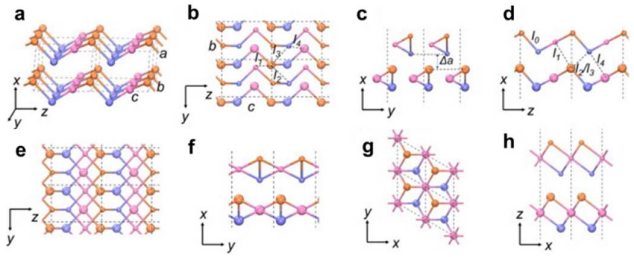

Figure 4 Structural allotropes for 2D Tellurium. (a-d) Crystal structures of bulk (a) and bilayer α-Te in the top- (b) and side-views (c, d); (e-f) Crystal structures of bilayer β-Te in the top- (e) and side-views (f); (g-h) Crystal structures of bilayer γ-Te in the top- (g) and side-views (h). Reproduced with permission from ref. 16. Copyright 2018, Elsevier.

3.2 Electronic bandstructure and carrier mobility in monolayer and few-layer tellurene

The electronic bandstructure in monolayer and few-layer tellurene has been recently explored using various theoretical schemes such as density functional theory (DFT)[14, 16, 17]. Ji and colleagues report an indirect bandgap of 1.17 eV for bilayer tellurene and an expected bandgap reduction with an increased layer thickness in the few-layer tellurene[16]. When the layer number of 2D Te increases, the valence band maximum (VBM) significantly changes from −4.98 to −4.35 eV, roughly three times that of the conduction band maximum (CBM), which suggests the formation of a *p*-type contact between few-layer tellurene with most metal electrodes. This is consistent with the device characteristics of field-effect transistors made from solution-grown tellurene[10]. Interestingly, the band structures of few-layer tellurene are predicted to have a four-fold valley degeneracy in the first Brillouin zone for the valence band, likely due to the (pseudo) spin non-degeneracy as a result of the strong spin-orbit coupling in Te[16]. Such "camel's back" shaped valence band is usually found in topological insulators with band inversion and play a key role for high-performance thermoelectrics[3]. By performing the hybrid DFT calculations, Zhu and colleagues predicted that the monolayer α- and β-tellurene exhibit indirect bandgaps of 1.15 and 1.79 eV, respectively[14]. The electronic gaps and band profiles for monolayer and few-layer tellurene have also been experimentally probed. Huang and co-workers report a gap of 0.92 eV for monolayer epitaxial tellurene on graphene[13] and a thickness-dependent bandgap evolution consistent with the theoretical predications[14, 16, 17]. The smaller monolayer bandgap observed could be due to the finite density of states of the underneath graphene near the Fermi level[13]. The scanning tunneling microscopy (STS) mapping of the real space band profiles shows that the epitaxial monolayer and few-layer tellurene are *p*-type semiconductors with the Fermi levels locating below the middle of the bandgap[13]. A similar bandgap evolution has also been reported for the epitaxial few-layer tellurene on HOPG substrate[33].

In addition to the thickness-dependent bandgap from mid-infrared to the red range which is of great interests to many emerging technologies in mid-infrared and terahertz applications, 2D Te has also been predicted to possess extraordinarily large room-temperature carrier mobilities ranging from hundreds to thousands of $cm^2V^{-1}s^{-1}$, much larger than those of 2D TMDCs and few-layer BP[14, 16]. Electrical characterization of the few-layer tellurene transistor devices yields hole mobilities consistent with the predicted ranges[10]. Such large room-temperature mobility in 2D Te is promising for constructing high-speed, energy-efficient electronics. An anisotropy in carrier mobility and electronic transport is expected for 2D Te, considering its structural anisotropy and the assumed different degrees of interaction along the Te chain directions (strong, covalent-type) and that between chains (weak, vdW-like)[35]. However, experiments have shown only a small degree of anisotropy (1.13) for few-layer tellurene[10]. Such an unexpected weak anisotropy in the electronic transport inspires a more profound understanding of the nature of the inter-chain interactions in 2D tellurene. Recent theoretical study[22] suggests that the delocalization of Te lone-pair electrons lowers the effective mass and changes the potential in the inter-chain region, hence enhancing the transport across the chains as well as the inter-chain interactions. The lone-pair electrons are delocalized by depletion of the density in their original positions and enhancement of the density in the inter-chain region, which adds "metallic bonding" or "covalent-like quasi-bonding" characteristics into the inter-chain interaction[16, 22]. This could also be understood by the relatively weak nucleus attraction and multi-valency nature of Te, which is a *metalloid* element with dual characteristics of both metal and nonmetal[14].

3.3 Optical properties and Raman Spectroscopy of 2D Te

Recent theoretical studies suggest a similar isotropic scenario for light absorption in few-layer tellurene[16], showing a strong broadband absorbance almost twice to three-times those of black phosphorus for the normal incident light linearly polarized along the two principal in-plane directions. Interestingly, the calculation results also indicate a layer-dependent absorbance that the absorption efficiency (i.e., the absorbance per layer) substantially increases with the decreased thickness of few-layer tellurene[16]. This is thought to be due to the thickness-dependent interlayer electronic hybridization and band dispersion, both of which become stronger as the layer thickness increases. This predicated high, isotropic optical-absorbance with the high mobility suggest the potential of tellurene for photonics and optoelectronics applications.

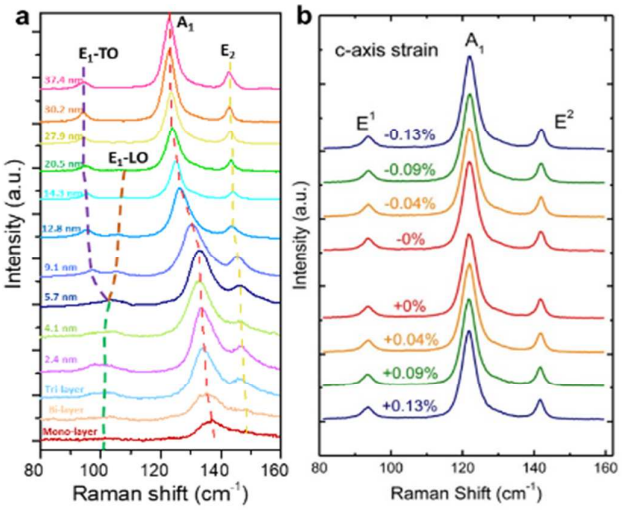

Figure 5 (a) Raman spectra for 2D Te with different thicknesses. Reproduced with permission from ref. 10. Copyright 2018, Springer Nature. (b) Raman spectra of Te thin film for both tensile and compressive c-axis strains. Reproduced with permission from ref. 11. Copyright 2017, American Chemical Society.

The fundamental light-matter interaction in 2D materials can also be probed and understood using spectroscopy techniques such as Raman scattering. In their recent report[10], Wu and colleagues performed the room-temperature angle-resolved polarized Raman spectroscopy for the solution-synthesized tellurene crystals with controlled thicknesses, and observed striking thickness-dependent variations (e.g., shifts, appearance, and disappearance) in Raman vibrational modes (Fig. 5a). For instance, the thick 2D Te samples (thicker than 20.5 nm) exhibit three Raman-active modes consistent with the previous observations in bulk and nanostructured tellurium[32, 36], indicating the "bulk" symmetric characteristics despite their 2D morphology. For the 2D tellurium crystals within the "intermediate" thickness range (e.g., 9.1 nm to 20.5 nm), the E_1 longitudinal (LO) phonons mode appears in the Raman spectra due to the deformation potential in tellurene lattice increases while the electro-optic effect weakens. When the 2D Te's thickness further reduces to few-layer ranges (smaller than 9.1 nm), the degeneracy in the E_1 transverse (TO) and longitudinal (LO) phonons occurs with peak broadening, possibly due to the thickness-dependent intra-chain atomic displacement, electronic band structure changes and symmetry assignments for each band. Also, significant peak shifts were also observed in the Raman Spectra, e.g., blue-shifts for A_1 and E_2 modes, when 2D tellurene's thickness decreases, which may be attributed to the enhanced interlayer interactions when thinned down. Such a peculiar behavior is thought to be closely related to the unique chiral-chain structure of tellurene. The effects of mechanical strains on the Raman spectroscopy for nanobelt-like 2D Te samples has further been studied, showing an anisotropic strain response along the two principal in-plane crystal directions (Fig. 5b)[11]. The theoretical Raman intensity of bi-layer tellurene as a function of vibrational frequency has also been recently reported[16], showing the splitting and anomalous shifts of frequency consistent with the experimental findings[10].

3.4 Magnetotransport in 2D Te

Bulk tellurium has been a material of interests for elucidating the fundamental quantum phenomena, e.g., scattering mechanisms of carriers, surface quantum states, magnetoresistance effect, quantum oscillation, topological insulator, and etc[4, 37, 38]. Recently, Du *et al*. carried out magnetotransport studies for the solution-synthesized 2D Te samples with magnetic fields applied along three principle axes[11]. The temperature-dependent phase coherence length extracted from the weak anti-localization effect (WAL) indicates its 2D transport behavior when an applied magnetic field is perpendicular to the $[10\bar{1}0]$ plane of 2D tellurene. The WAL effect vanishes with the applied magnetic field parallel to the $<1\bar{2}10>$ direction (perpendicular to the Te chains). When the applied magnetic field is along the <0001> chain direction of 2D Te, the corresponding phase coherence length extracted from the universal conductance fluctuations (UCF) indicates the nature of 1D transport mechanism. The atomically thin 2D Te crystal with its intriguing properties is expected to provide an attractive platform for exploring the quantum physics at the frontier of condensed matter research.

3.5 Environmental stability of 2D Te

The environmental instability of many 2D materials, e.g., black phosphorus, has severely limited the application prospects of related materials. In sharp contrast, great air-stability has been demonstrated in solution-grown 2D Te crystals for almost the entire thickness range from thick flakes down to a few-layer thickness. No significant degradation has been observed in the electrical performance of the prototypical 2D tellurene transistors that were exposed in air for two months without any encapsulation[13]. Theoretical studies suggest that an energy barrier exists for the related oxidation pathways, sufficient to prevent the few-layer tellurene being oxidized under ambient conditions. Such good environmental stability is critical for exploring the fundamental properties and realizing the technological prospects of 2D tellurene.

4. Device applications of 2D Te

4.1 2D tellurene field-effect transistors

Wu *et al.* demonstrated the prototypical 2D tellurene field-effect transistors (FETs) with a good all-around figure of merits compared to known 2D materials[10]. The long channel devices

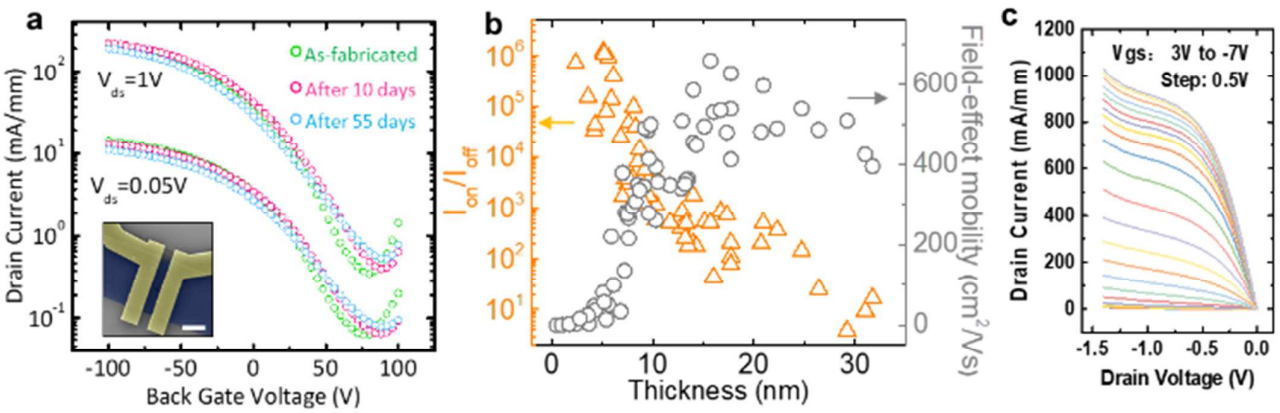

Figure 6 2D tellurene FET performance. (a) Transfer curves of a typical 2D tellurene transistor with a thickness of 15 nm and stability measured for 55 days. (Inset: False-colored SEM image of a tellurene transistor. The scale bar is 10 μm.); (b) Thickness-dependent on/off ratio (orange triangles) and field-effect mobility (gray circles) for 2D Te transistors; (c) High on-state current density in a 11.1-nm-thick short-channel tellurene transistor with 300-nm channel. Reproduced with permission from ref. 10. Copyright 2018, Springer Nature.

(channel length 3 μm) exhibit large drain current over 300 mA/mm, high room-temperature mobility ~700 cm^2/Vs, and high on/off ratio on the order of ~10^5 (Fig. 6). The thickness dependence of on/off ratios and field-effect mobilities in 2D tellurene long channel devices with thicknesses ranging from over 35 nm down to a monolayer (~0.5 nm) has also been explored to elucidate the transport mechanism of 2D Te FETs. A benchmark comparison with black phosphorus shows that the solution-synthesized 2D tellurene has ~ 2-3 times higher mobility than black phosphorus when the same device structure, geometry, and mobility extraction method are adopted. By further exploring the channel scaling and integration with atomic-layer-deposition (ALD) grown high-k dielectric for the 2D tellurene transistors, Wu and colleagues achieved record high drive current of over 1 A/mm and good on/off ratios ~ 10^3 at relatively low drain bias[10]. The maximum drain current achieved is 1.06 A/mm, which is comparable to that of conventional semiconductor devices and the highest value among all 2D material transistors. This is significant for potential design and implementation of high-performance tellurene-based electronics. The in-plane electrical transport along different crystal directions was also studied at room temperature, and the average anisotropic mobility ratio is 1.43±0.10, which is slightly lower than the reported values for bulk tellurium[35], possibly due to the enhanced surface scattering in our ultrathin Te samples.

5. Conclusions and Outlook

Despite being one of the newest members to the 2D materials family, 2D tellurene has attracted numerous interests for its intriguing, versatile material properties and technological potential, ushering in new research opportunities in both the theoretical and experimental studies. Tellurene possesses a few unique characteristics and advantages compared to the state-of-the-art 2D materials. For instance, the negligible bandgap of graphene leads to compromised power gains and limited applications for energy-efficient electronics, while tellurene has a process-modulated bandgap (~0.35-1.2 eV from mid-IR to visible light); transition metal dichalcogenides' low room-temperature mobilities limit their prospects for high-speed devices, while tellurene possesses a high room-temperature carrier mobility (~10^3 cm^2/Vs); the air-instability of silicene and black phosphorous limit their potential for practical applications, while tellurene shows a good air-stability for almost the entire thickness range. In terms of synthesis control, free-standing tellurene with large lateral dimensions (~100 μm) and process-controlled thickness (from a monolayer to tens of nm) can be scalably produced with high yield (> 95%). Nevertheless, the majority of efforts in the state-of-the-art 2D materials are restricted by factors such as growth substrates, synthetic conditions, and small crystal size of the obtained materials. For instance, top-down liquid-phase exfoliation show potential in producing large quantities of various atomically-thin layered materials, e.g., graphene, transition metal dichalcogenides, and boron nitride. However, the poor control in thickness uniformity and small size of derived materials undermine the viability of such approaches. The bottom-up chemical vapor deposition process can lead to high-quality crystals of graphene and MoS_2 with controlled thickness over a large area. However, the requirement for high growth temperature and delicate control in growth atmosphere limit the potential for scale-up. Epitaxy growth of 2D materials with exotic properties, e.g., silicene, borophene, and stanene, have also been explored, though proved challenging due to the process-inherent requirements for epitaxy substrates and high vacuum. Still, much work remains to be done to attain a comprehensive fundamental understanding of tellurene's properties and to realize its full potential, with the following opportunities and challenges.

Fundamental exploration: Recent theoretical studies suggest that few-layer tellurene is highly stretchable along the Te chain direction[16]. This could enable high-performance flexible and stretchable devices with good lifetime and mechanical durability using the solution-grown 2D tellurene, through scalable assembly and integration approaches, e.g., ink-jet printing[13]. Despite being an elemental material, the trigonal Te lacks the centrosymmetry in its crystal structure and has hence been predicted to exhibit piezoelectricity[39]. Nevertheless, few studies have been reported on Te's piezoelectric property, possibly due to the narrow bandgap of bulk Te. The reduction of dimensionality in tellurene could lead to strong, accessible piezoelectricity compared to its bulk

counterpart[12]. The exploration of tellurene's piezoelectricity is potentially significant in the sense that the origin for tellurene's piezoelectric characteristics is expected to be fundamentally different from the ion polarization process for the known piezoelectric materials[40, 41]. Furthermore, the coupling of tellurene's piezoelectricity with its appealing semiconductor characteristics suggests the potential of 2D tellurene as good candidate material platform for emerging areas such as piezotronics and piezo-phototronics[42-44]. The absence of inversion symmetry combined with the strong spin-orbit interaction in manufacturable 2D tellurene may also offer interesting opportunities in exploring the manipulation of the valley degree of freedom for practical valleytronics devices[45]. Moreover, due to the lack of inversion symmetry, the spin splitting of the bulk band could give rise to a current-induced magnetization in the nonmagnetic bulk tellurium[46]. It would, therefore, be interesting to explore the feasibility of 2D tellurene as a new class of magnetoelectric material which could potentially exhibit both the current-induced spin magnetization and current-induced orbital magnetization[47], considering as well the chiral nature of 2D tellurene[3, 4]. A recent theoretical work also predicted that few-layer tellurene surprisingly exhibits in-plane ferroelectricity due to the interlayer interaction between lone pairs[19]. This coupled with the nontrivial valley-dependent spin-textures for holes in few-layer tellurene could enable novel electronic and spintronic applications. The anisotropic and layer-dependent electron and hole pockets found for few-layer tellurene[16] indicate that 2D tellurene possess more suitable electronic structures than that of 1D Te nanostructures for high-performance thermoelectric devices[20, 21]. For the electronic device applications, it is expected that the mobility of tellurene can be further improved through approaches such as improving interface quality with high-k dielectric or h-BN encapsulation to reduce the substrate phonon scattering and charge impurity. Meanwhile, a comprehensive examination of the interfacial characteristics between 2D tellurene and electrode materials is necessary for providing the fundamental understandings, e.g., the effects of metals and electrode configurations on the carrier transport in the metal-tellurene contact[23]. Such knowledge is critical for the rational design and optimization of future tellurene-based devices. The exploration of the fundamental doping mechanism and defect chemistry in 2D tellurium is essential for not only providing versatility in modulating its material properties by design but may also enable novel device concepts and applications. All these intriguing properties demonstrate 2D tellurene a highly promising elementary 2D semiconductor for diverse applications and inspire us to explore the novel physics and unusual phenomena in the relatively unchartered areas of 2D non-layered materials, in particular, those with the structural similarity to 2D tellurene and consist of weakly bonded atomic chains[48, 49].

Technological implementation: Among all the demonstrated approaches to synthesize Te nanostructures, as have been reviewed in the previous sections, hydrothermal processing emerges as a potential economic method for nanomanufacturing 2D tellurene, due to its energy saving, cost-effectiveness, low working temperature, feasibility for scale-up production, and the potential for deriving 2D tellurene with uniform thickness and dimensions. The room-temperature air-stability of 2D Te crystals also makes it feasible and convenient to produce, package, transportation, and utilization of the as-fabricated 2D Te materials. The as-fabricated tellurene could also be used as templates for deriving large-area, free-standing 2D tellurides with tailored dimensions and properties[50] as well as a versatile class of heterostructures for functional devices. In order to realize the manufacturing and production potential of solution-synthesized 2D Te, more efforts are required to reveal and identify the scientific nature of hydrothermal processing for 2D Te, particularly on the spatial distribution of nucleation and growth, patterning, and self-assembly into device forms, which directly impact the growth rate, assembly yield, performance uniformity, and batch-to-batch reproducibility for future practical production and application of 2D tellurene.

The rapid and exciting progress achieved in many emerging and "traditional" disciplines, e.g., nanomanufacturing, data science, condensed matter physics, material science, solid-state chemistry, and etc, are expected to excite a confluence of collective efforts from the research community and lead to more theoretical/experimental advances in probing the fundamental properties of the 2D tellurene and implementing novel devices. 2D tellurene adds a new class of nanomaterials to the large family of 2D crystals.

Conflicts of interest

There are no conflicts to declare.

Acknowledgments

W. Z. W. acknowledges the College of Engineering and School of Industrial Engineering at Purdue University for the startup support. W. Z. W. was partially supported by the Oak Ridge Associated Universities (ORAU) Junior Faculty Enhancement Award Program. W. Z. W. was partially sponsored by the National Science Foundation under grants CMMI- 1663214 and CNS-1726865. W. Z. W. and P. D. Y. were partially supported by Army Research Office under grant no. W911NF-15-1-0574 and W911NF-17-1-0573. P. D. Y. was supported by NSF/AFOSR 2DARE Program and SRC.

Notes and references

1. V. E. Bottom, *Science*, 1952, **115**, 570.
2. J.-W. Liu, J.-H. Zhu, C.-L. Zhang, H.-W. Liang and S.-H. Yu, *Journal of the American Chemical Society*, 2010, **132**, 8945-8952.
3. H. Peng, N. Kioussis and G. J. Snyder, *Physical Review B*, 2014, **89**, 195206.
4. L. A. Agapito, N. Kioussis, W. A. Goddard and N. P. Ong, *Physical Review Letters*, 2013, **110**, 176401.
5. D. Souilhac, D. Billerey and A. Gundjian, *Applied Optics*, 1990, **29**, 1798-1804.
6. A. von Hippel, *The Journal of Chemical Physics*, 1948, **16**, 372-380.

7. B. Mayers and Y. Xia, *Journal of Materials Chemistry*, 2002, **12**, 1875-1881.
8. M. Mo, J. Zeng, X. Liu, W. Yu, S. Zhang and Y. Qian, *Advanced Materials*, 2002, **14**, 1658-1662.
9. H.-S. Qian, S.-H. Yu, J.-Y. Gong, L.-B. Luo and L.-f. Fei, *Langmuir*, 2006, **22**, 3830-3835.
10. Y. Wang, G. Qiu, R. Wang, S. Huang, Q. Wang, Y. Liu, Y. Du, W. A. Goddard, M. J. Kim, X. Xu, P. D. Ye and W. Wu, *Nature Electronics*, 2018, **1**, 228-236.
11. Y. Du, G. Qiu, Y. Wang, M. Si, X. Xu, W. Wu and P. D. Ye, *Nano Letters*, 2017, **17**, 3965-3973.
12. W. Shengjie Gao and Yixiu Wang and Ruoxing Wang and Wenzhuo, *Semiconductor Science and Technology*, 2017, **32**, 104004.
13. X. Huang, J. Guan, Z. Lin, B. Liu, S. Xing, W. Wang and J. Guo, *Nano Letters*, 2017, **17**, 4619-4623.
14. Z. Zhu, X. Cai, S. Yi, J. Chen, Y. Dai, C. Niu, Z. Guo, M. Xie, F. Liu, J.-H. Cho, Y. Jia and Z. Zhang, *Physical Review Letters*, 2017, **119**, 106101.
15. M. A. a. A. R. Lede Xian and Alejandro Pérez Paz and Elisabeth Bianco and Pulickel, *2D Materials*, 2017, **4**, 041003.
16. J. Qiao, Y. Pan, F. Yang, C. Wang, Y. Chai and W. Ji, *Science Bulletin*, 2018, **63**, 159-168.
17. L. Bozhao Wu and Xinghui Liu and Jiuren Yin and Hyoyoung, *Materials Research Express*, 2017, **4**, 095902.
18. X. H. Wang, D. W. Wang, A. J. Yang, N. Koratkar, J. F. Chu, P. L. Lv and M. Z. Rong, *Physical Chemistry Chemical Physics*, 2018, **20**, 4058-4066.
19. Y. Wang, C. Xiao, M. Chen, C. Hua, J. Zou, C. Wu, J. Jiang, S. A. Yang, Y. Lu and W. Ji, *Materials Horizons*, 2018, **5**, 521-528.
20. S. Sharma, N. Singh and U. Schwingenschlögl, *ACS Applied Energy Materials*, 2018, **1**, 1950-1954.
21. Z. Gao, F. Tao and J. Ren, *Nanoscale*, 2018.
22. Y. Liu, W. Wu and W. A. Goddard, *Journal of the American Chemical Society*, 2018, **140**, 550-553.
23. J. Yan, X. Zhang, Y. Pan, J. Li, B. Shi, S. Liu, J. Yang, Z. Song, H. Zhang, M. Ye, R. Quhe, Y. Wang, J. Yang, F. Pan and J. Lu, *Journal of Materials Chemistry C*, 2018.
24. Z. Tang, Y. Wang, K. Sun and N. A. Kotov, *Advanced Materials*, 2005, **17**, 358-363.
25. T. Yang, H. Ke, Q. Wang, Y. a. Tang, Y. Deng, H. Yang, X. Yang, P. Yang, D. Ling, C. Chen, Y. Zhao, H. Wu and H. Chen, *ACS Nano*, 2017, **11**, 10012-10024.
26. H. Muhammad Safdar and Xueying Zhan and Mutong Niu and Misbah Mirza and Qing Zhao and Zhenxing Wang and Jinping Zhang and Lianfeng Sun and Jun, *Nanotechnology*, 2013, **24**, 185705.
27. X.-L. Li, G.-H. Cao, C.-M. Feng and Y.-D. Li, *Journal of Materials Chemistry*, 2004, **14**, 244-247.
28. O. Noboru Furuta and Hideki Itinose and Nobuyuki Maruyama and Yosio, *Japanese Journal of Applied Physics*, 1972, **11**, 1113.
29. W. Noboru Furuta and Norio, *Japanese Journal of Applied Physics*, 1972, **11**, 1753.
30. Z. Baoyou Geng and Yu Lin and Xingsheng Peng and Guowen Meng and Lide, *Nanotechnology*, 2003, **14**, 983.
31. Z. He, Y. Yang, J.-W. Liu and S.-H. Yu, *Chemical Society Reviews*, 2017, **46**, 2732-2753.
32. Q. Wang, M. Safdar, K. Xu, M. Mirza, Z. Wang and J. He, *ACS Nano*, 2014, **8**, 7497-7505.
33. J. Chen, Y. Dai, Y. Ma, X. Dai, W. Ho and M. Xie, *Nanoscale*, 2017, **9**, 15945-15948.
34. Z. Xie, C. Xing, W. Huang, T. Fan, Z. Li, J. Zhao, Y. Xiang, Z. Guo, J. Li, Z. Yang, B. Dong, J. Qu, D. Fan and H. Zhang, *Advanced Functional Materials*, 2018, **28**, 1705833.
35. L. Rothkirch, R. Link, W. Sauer and F. Manglus, *physica status solidi (b)*, 1969, **31**, 147-155.
36. A. Pine and G. Dresselhaus, *Physical Review B*, 1971, **4**, 356.
37. K. von Klitzing and G. Landwehr, *Solid State Communications*, 1971, **9**, 2201-2205.
38. K. Nakayama, M. Kuno, K. Yamauchi, S. Souma, K. Sugawara, T. Oguchi, T. Sato and T. Takahashi, *Physical Review B*, 2017, **95**, 125204.
39. G. Arlt and P. Quadflieg, *physica status solidi (b)*, 1969, **32**, 687-689.
40. W. Wu, X. Wen and Z. L. Wang, *Science*, 2013, **340**, 952-957.
41. W. Wu, L. Wang, Y. Li, F. Zhang, L. Lin, S. Niu, D. Chenet, X. Zhang, Y. Hao, T. F. Heinz, J. Hone and Z. L. Wang, *Nature*, 2014, **514**, 470-474.
42. W. Wu and Z. L. Wang, *Nature Reviews Materials*, 2016, **1**.
43. Z. L. Wang and W. Z. Wu, *National Science Review*, 2014, **1**, 62-90.
44. Z. L. Wang, *Piezotronics and Piezo-Phototronics*, Springer, 2012.
45. J. R. Schaibley, H. Yu, G. Clark, P. Rivera, J. S. Ross, K. L. Seyler, W. Yao and X. Xu, *Nature Reviews Materials*, 2016, **1**, 16055.
46. T. Furukawa, Y. Shimokawa, K. Kobayashi and T. Itou, *Nature Communications*, 2017, **8**, 954.
47. T. Yoda, T. Yokoyama and S. Murakami, *Scientific Reports*, 2015, **5**, 12024.
48. G. Liu, B. Debnath, T. R. Pope, T. T. Salguero, R. K. Lake and A. A. Balandin, *Nature Nanotechnology*, 2016, **11**, 845.
49. J. O. Island, A. J. Molina-Mendoza, M. Barawi, R. Biele, E. Flores, J. M. Clamagirand, J. R. Ares, C. Sánchez, Herre SJ van der Zant, R. D'Agosta, I. J. Ferrer, A. Castellanos-Gomez, *2D Materials*, 2017, **4**, 022003.
50. G. D. Moon, S. Ko, Y. Min, J. Zeng, Y. Xia and U. Jeong, *Nano Today*, 2011, **6**, 186-203.